Layered Structures

Deutsche Ausgabe: DOI: 10.1002/ange.201506152
Internationale Ausgabe: DOI: 10.1002/anie.201506152

Designed Synthesis of van der Waals Heterostructures: The Power of Kinetic Control

Matti B. Alemayehu, Matthias Falmbigl, Kim Ta, Jeffrey Ditto, Douglas L. Medlin, and David C. Johnson**

Abstract: *Selecting specific 2D building blocks and specific layering sequences of van der Waals heterostructures should allow the formation of new materials with designed properties for specific applications. Unfortunately, the synthetic ability to prepare such structures at will, especially in a manner that can be manufactured, does not exist. Herein, we report the targeted synthesis of new metal–semiconductor heterostructures using the modulated elemental-reactant technique to nucleate specific 2D building blocks, control their thickness, and avoid epitaxial structures with long-range order. The building blocks, VSe_2 and $GeSe_2$, have different crystal structures, which inhibits cation intermixing. The precise control of this approach enabled us to synthesize heterostructures containing $GeSe_2$ monolayers alternating with VSe_2 structural units with specific sequences. The transport properties systematically change with nanoarchitecture and a charge-density wave-like transition is observed.*

The discovery of graphene in 2004 and subsequent preparation of isolated monolayers of layered materials, such as *h*BN and transition-metal dichalcogenides, have had a profound effect on the fields of condensed-matter physics and materials science.[1–4] Mechanical exfoliation, chemical isolation, and van der Waals epitaxy via vapor deposition have all been shown to yield 2D structures.[3,5–9] The next big advance was the creation of heterostructures by stacking different 2D crystals on top of each other in a chosen sequence, creating artificial materials.[10,11] To form these van der Waals heterostructures, two 3D van der Waals compounds (such as graphite, $MoSe_2$, $NbSe_2$, WSe_2 …) are typically cleaved at their van der Waals gap and placed on top of one another to form novel heterostructures. Heterostructures open a pathway to materials by design and offer potentially enhanced performance in many applications including energy conversion and storage, catalysis, sensing, and memory devices.[12–16]

The major challenges in forming van der Waals heterostructures were recently summarized by Geim and Grigorieva.[17] They provided "three rules of survival" to guide this growing field: 1) the parent 3D structure should have a melting temperature above 1000 °C so that the 2D sheet is stable at room temperature, 2) the 3D structure must be chemically inert so that no decomposed surface layer forms in air or any other environment, 3) insulating and semiconducting 2D-crystals are more likely to be stable compared to metallic ones. Other challenges for scientists in this field include avoiding epitaxial relationships between the 2D structures and the substrate and precisely controlling the chosen sequence and thickness of the constituent layers of the heterostructure.

The modulated elemental-reactants (MER) technique provides a way to overcome these challenges. The MER approach precisely controls the layer sequence and nanoarchitecture of intergrowths of a transition-metal dichalcogenide and a rock salt structured constituent by using designed precursors where no epitaxial relationship between the constituents or the substrate exists.[18,19] Herein we show the successful synthesis of heterostructures of VSe_2 (metallic) and $GeSe_2$ (layered semiconductor with melting point of 742 °C), which violate the survival rules outlined by Geim and Grigorieva. Bulk $GeSe_2$ has a GeS_2-type crystal structure with *a*-, *b*-, *c*-lattice parameters and β of 0.7016(5) nm, 1.6796(8) nm, 1.1831(5) nm and 90.65(5)° respectively,[20] and was reported to have strong covalent bonding within the corrugated $GeSe_2$ sheets. Bulk VSe_2 crystallizes in a 1*T* polytype[21] and is among the most thoroughly investigated transition-metal dichalcogenides owing to its charge-density wave transition with an onset temperature of 100 K.[22–24] The different structure types makes intermixing of Ge and V less likely.[25] To our knowledge, $GeSe_2$ has not been considered as a potential candidate for forming heterostructures.[17] As a member of the IV–VI family of semiconductors, bulk $GeSe_2$ has a wide band gap (ca. 2.3 eV) and has potentially promising applications in electronics, optoelectronics, and renewable energy devices. There are limited reports of nanostructured $GeSe_2$ in the literature.[26–30]

To prepare the targeted intergrowth structures, we deposited specific sequences of bilayers of Ge and Se and bilayers of V and Se in 1:2 atomic ratios onto a silicon or quartz substrate via physical vapor deposition (PVD). An iterative calibration process was carried out to obtain 1:2 ratios of Ge and V to Se within each of the bilayers, and to obtain the targeted misfit ratio between these two different bilayers.[31] The precursors were self-assembled into the targeted metastable compounds by a short low-temperature annealing process (Figure 1 a). By varying the number of each of the bilayers deposited, the compounds $VSe_2(m)$–$GeSe_2(n)$, where $m = 2$–4 and $n = 1$ and $m = 3$, $n = 2$, were synthesized. Throughout the manuscript we identify the compounds with a short-hand notation of (m,n) indicating the number of

[*] Dr. M. B. Alemayehu, Dr. M. Falmbigl, K. Ta, J. Ditto, Dr. D. C. Johnson
Department of Chemistry
University of Oregon
Eugene, OR 97403 (USA)
E-mail: matti@uoregon.edu
davej@uoregon.edu
Dr. D. L. Medlin
Sandia National Laboratories
7011 East Avenue, MS 9161, Livermore, CA 94551 (USA)

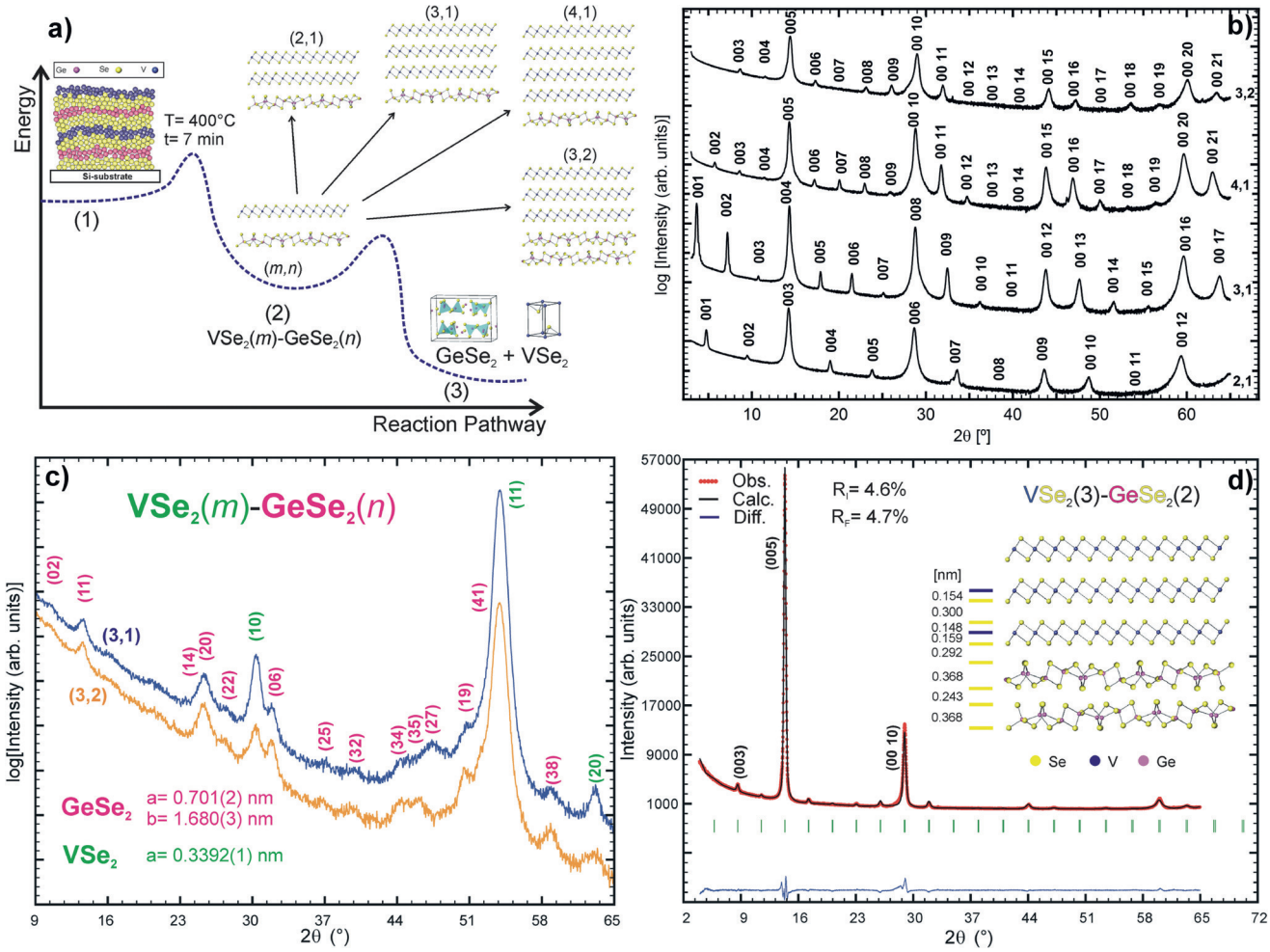

Figure 1. Structural information for the VSe_2–$GeSe_2$ heterostructures. a) Energetic requirements and reaction pathway for the formation of the $VSe_2(m)$–$GeSe_2(n)$ heterostructures where $m = 2$–4 and $n = 1$–2. b) Specular X-ray diffraction patterns of $VSe_2(m)$–$GeSe_2(n)$. c) In-plane X-ray diffraction patterns of $VSe_2(3)$–$GeSe_2(1)$ and $VSe_2(3)$–$GeSe_2(2)$. d) Rietveld refinement of $VSe_2(3)$–$GeSe_2(2)$, the error of atomic plane distances is below 0.002 nm.

(VSe_2, $GeSe_2$) layers, respectively (Figure 1a). Figure 1b shows the specular X-ray diffraction patterns of the compounds where $n = 1$–2 and $m = 2$–4, which contain only (00*l*) reflections. The calculated *c*-lattice parameters increase by 0.609(2) nm per VSe_2 layer, which is close to that reported for intergrowths of VSe_2 with rock salt structured constituents.[32] The $GeSe_2$ layer adds 0.670(4) nm (i.e. the thickness of a $GeSe_2$ monolayer) to the *c*-lattice parameter of the (*m*,1) compounds. In the (3,2) compound, the thickness of the bilayer $GeSe_2$ was calculated to be 1.125(6) nm, which is close to the *c*-lattice parameter of bulk $GeSe_2$.[20]

To gain more insight into the structural arrangement of the heterostructures, Rietveld refinements of the 00*l* reflections for the (3,1) and (3,2) compounds were conducted (Figure 1d). Fixing the atomic plane distances for the $GeSe_2$ to those found in the bulk compound, the atomic planes of the VSe_2 and the van der Waals gap distances between the layers were refined yielding the distances between atomic planes along the *c*-axis. The

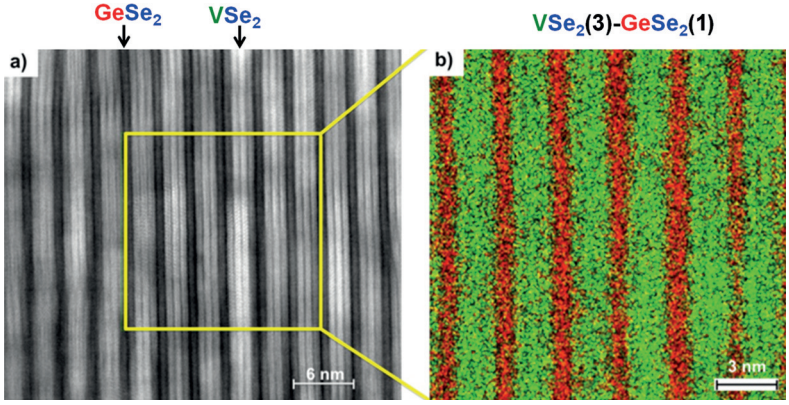

Figure 2. STEM image and an EDX map of the (3,1) heterostructure. a) STEM image of the $VSe_2(3)$–$GeSe_2(1)$ compound with VSe_2 corresponding to the bright layers and $GeSe_2$ corresponding to the dark layers. b) EDX map of the area highlighted by the yellow square in (a). Ge red, V green.

resulting van der Waals gaps are VSe_2–VSe_2: 0.300(2) nm; VSe_2–$GeSe_2$: 0.292(2) nm; and $GeSe_2$–$GeSe_2$: 0.243-(2) nm. The $GeSe_2$–$GeSe_2$ gap is larger than the bulk value (0.213 nm)[20] and the VSe_2–VSe_2 distance is similar to its bulk counterpart (0.297–0.306 nm)[21,33] (Figure 1d). These results indicate that the heterostructures contain monolayers of $GeSe_2$.

In-plane X-ray diffraction supports the structural refinement, containing reflections consistent with the presence of independent crystal structures for both constituents. Indexing the reflections shows that specific planes of both constituents are parallel to one another and are crystallographically aligned to the substrate. The in-plane lattice parameters, given in Figure 1c, are in good agreement with those of the bulk compounds,[20,33] which supports the interpretation of minimal cation intermixing across the interfaces. The lattice mismatch along the *a*- and *b*-axis and different in-plane geometries (hexagonal and monoclinic) reinforce that this synthesis technique does not require an epitaxial relationship between the constituents.

Further confirmation of the formation of distinct VSe_2 and $GeSe_2$ layers is provided by transmission electron microscopy. Figure 2a shows a high-angle annular dark field (HAADF) scanning transmission electron microscopy (STEM) image of VSe_2(3)–$GeSe_2$(1) showing the clearly distinguishable layers. The corresponding energy dispersive X-ray spectroscopy (EDX) maps for Ge and V in Figure 2b demonstrate the strong partitioning of the cations to their specific layers.

Additional insights concerning the structure of these new compounds containing thin slabs of $GeSe_2$ are provided by the HAADF-STEM images of the (3,1) heterostructure shown in Figure 3 and Figure 4. In Figure 3b, a cross-sectional view of the entire film is presented with a total film thickness of 50 nm corresponding to 20 structural units. Continuous stacking of three VSe_2 layers (bright in Figure 3b) followed by a single $GeSe_2$ layer (dark in Figure 3b) is found throughout the sample, without any stacking defects and with atomically sharp interfaces between the constituents. Several different crystallographic orientations between subsequent layers were found indicating rotational disorder. Similar disorder was found in previous compounds synthesized via the MER technique.[18]

Figure 4a highlights a region of the STEM image with a [100] zone axis orientation of $GeSe_2$, and the *b*- lattice parameter of 1.70(5) nm, which is consistent with the in-plane

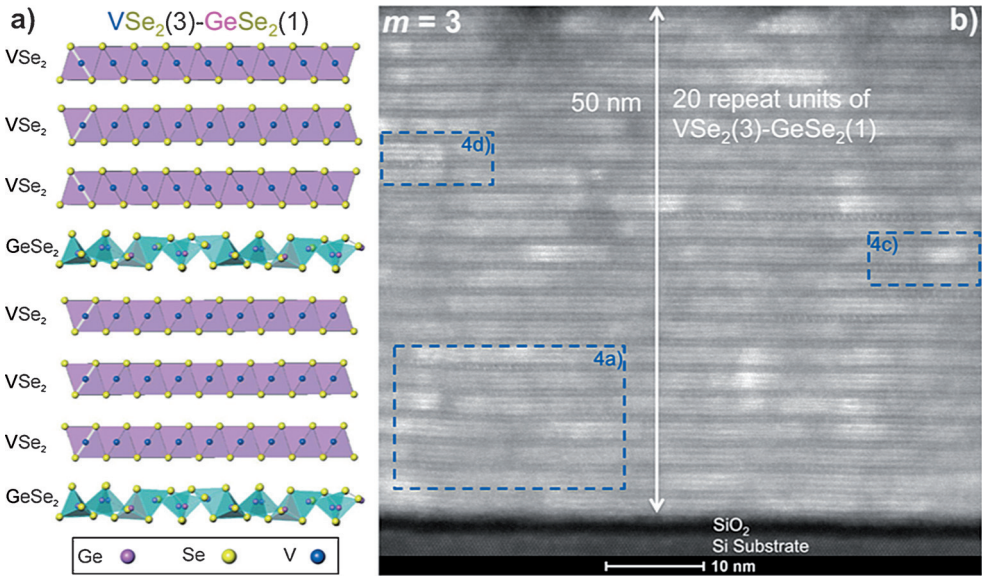

Figure 3. Superlattice structural representation and HAADF-STEM image of the (3,1) heterostructure. a) Two structural units of the VSe_2(3)–$GeSe_2$(1) compound highlighting rotational disorder indicated by white marks. b) HAADF-STEM image of VSe_2(3)–$GeSe_2$(1) with all the 20 consecutive structural units of the (3,1) compound. The highlighted areas labeled 4a, 4c, and 4d refer to the close up images in Figure 4.

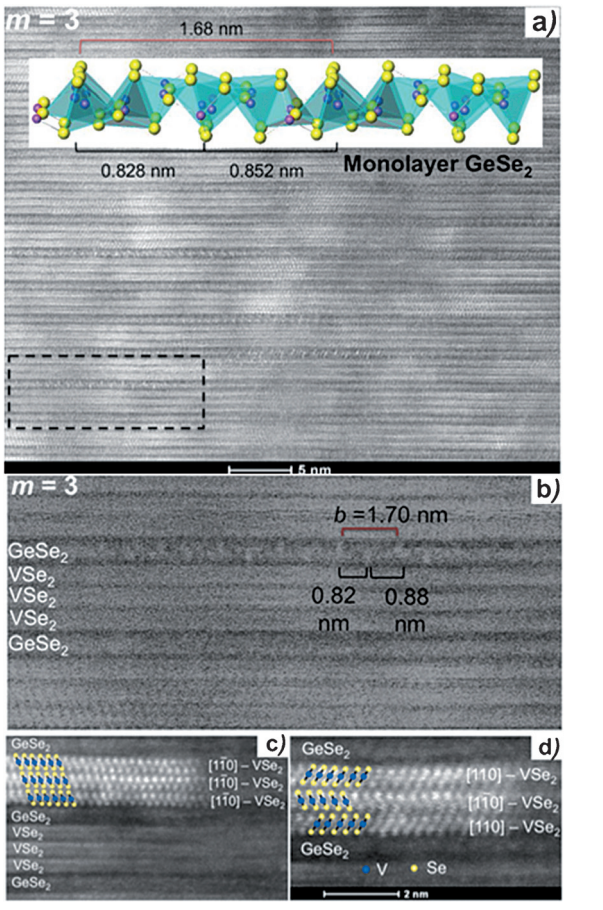

Figure 4. HAADF-STEM images of the (3,1) heterostructure. a) A monolayer $GeSe_2$ structure with a section that contains the $GeSe_2$ structure shown. b) An enlargement of Figure 4a illustrating the [100] orientation of the $GeSe_2$ structure. An enlargement of Figure 3b where the same (c) or different (d) VSe_2 orientations are observed.

X-ray diffraction discussed above. The periodicities of the observed intensity modulations are consistent with those expected from a [100] oriented slice of the bulk structure (see inset of Figure 4a). This supports our assertion that a monolayer of $GeSe_2$ is incorporated into these new compounds. Regions of the VSe_2 layers down the [110] zone axis are consistent with a Se-V-Se trilayer with V in octahedral coordination (Figure 4c). A close inspection of the VSe_2 layers contains regions that are not stacked as expected for a 1*T*-polytype (Figure 4d). To our knowledge this has never been observed before, and highlights the rotational disorder between layers in these new compounds.

All the VSe_2–$GeSe_2$ heterostructures exhibit metallic behavior, agreeing with theoretical calculations by Terrones that predict metal–semiconductor heterostructures to exhibit metallic behavior.[34] A significant change of the magnitude as well as the temperature dependence of the resistivity is observed as the ratio of the constituents is varied (Figure 5a). The resistivity increases with the content of $GeSe_2$ per repeat unit as would be expected for a larger amount of the semiconducting component. All of the compounds exhibit an anomaly, which changes in magnitude and onset temperature systematically with the amount of $GeSe_2$ per repeat unit. The magnitude of the anomaly is much larger than the charge-density wave transition observed in bulk VSe_2 or any reported VSe_2 nanostructures. For the (2,1) compound, an increase in the resistivity by a factor of two is observed, which is higher than reported for the charge density wave in VSe_2 containing intergrowth compounds.[32]

To get deeper insight into the observed changes in electrical resistivity, Hall effect measurements were conducted (Figure 5b). While bulk VSe_2 has a small negative Hall coefficient at room temperature, owing to its nearly half filled d-band, all the VSe_2–$GeSe_2$ compounds have a positive Hall coefficient at room temperature suggesting charge transfer from $GeSe_2$ to VSe_2 has occurred. The Hall coefficient of bulk VSe_2 becomes increasingly negative with an abrupt change in slope at the charge-density wave onset temperature of 100 K.[22] The Hall coefficients of the (3,1) and (4,1) compounds linearly decrease as temperature is decreased, changing sign at about 175 K with a change in slope at 150 K and 100 K, similar to that of bulk VSe_2 respectively. These changes correlate with the observed increases in resistivity at around 130 K and 100 K observed in the (3,1) and (4,1) compounds respectively. The change in sign of the Hall coefficient indicates that both electrons and holes contribute to the conductivity. The sign of R_H for the (2,1) compound remains positive throughout the temperature range investigated and shows a sharp increase at the same temperature where the resistivity increases, also suggesting that carriers are localized as would be expected in a charge-density wave. This evolution, as the thickness of the VSe_2 constituent layer decreases, highlights the sensitivity of properties to the nanoarchitecture of the layering sequence. Examining R_H for the (3,2) compound allows us to begin to separate the effect of constituent thickness from the ratio of constituents. The sign of R_H is positive but an order of magnitude smaller than observed for the (2,1) compound. There is a smooth increase by an order of magnitude in R_H as temperature is decreased between 150 K and 100 K. Again, the change in R_H corresponds to the observed increase in the resistivity. Comparing the Hall coefficients at low temperatures reveals electrons and holes as majority carrier types for the heterostructures with n/m ratio below and above 0.35 respectively (Figure 5c). This further indicates that with increasing content of $GeSe_2$, the electronic structure of the heterostructures is significantly altered from that of bulk VSe_2.[35]

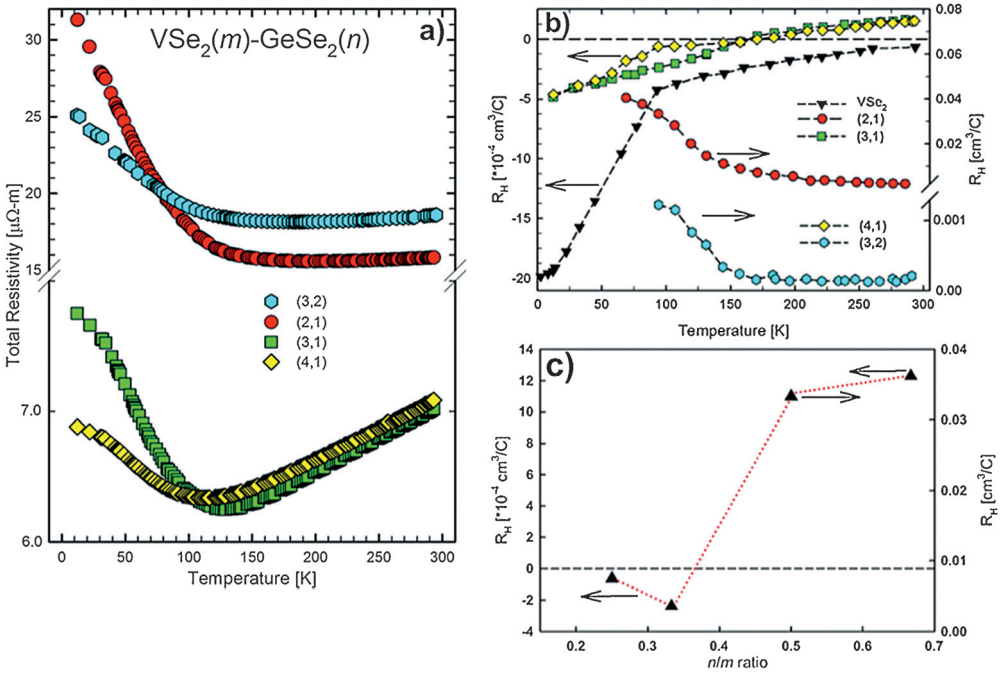

Figure 5. Electrical transport properties of $VSe_2(m)$–$GeSe_2(n)$ where $m = 2$–4 and $n = 1$ or 2. a) Temperature-dependent resistivity. Note: the break in the *y*-axis. b) Temperature dependent Hall coefficient. Note: the scale change in the *y*-axis. c) Hall coefficient at 95 K as a function of n/m ratio.

In conclusion, metal–semiconductor heterostructures were synthesized via the MER technique. Different crystal structures were incorporated into the heterostructure to avoid the pitfall of intermixing of cations in heterostructures with the same crystal structures. The precise control afforded by the synthesis technique allowed the formation of the first monolayer of $GeSe_2$ ever reported. The transport properties show systematic changes as a function of both VSe_2 and $GeSe_2$ content. Compared to bulk VSe_2 the charge-density wave-like transition is strongly enhanced and the transition temperature and

magnitude of this anomaly can be tuned by varying the layering sequence. This example demonstrates that the MER technique provides a powerful alternative to other synthesis methods and allows several present limitations to a set of materials accessible for van der Waals heterostructures to be overcome, such as cation intermixing across constituents, epitaxial relationships, restriction to semiconducting and insulating constituents, and formation of a limited number of sheets of the heterostructure compounds.

Experimental Section

We used the modulated elemental reactant (MER) technique to synthesize the compounds reported via physical vapor deposition. The sequential deposition technique which requires an extensive calibration is described in detail elsewhere.[36]

Specular and in-plane X-ray diffraction measurements were performed on a Bruker AXS D8 diffractometer and Rigaku SmartLab equipped with $Cu_{K\alpha}$ (0.154 nm) radiation, respectively. High angular annular dark field scanning transmission electron microscopy (HAADF-STEM) samples were prepared on an FEI Helios Nanolab 600 Dual Beam focused ion beam (FIB) using a method developed by Schaffer et al.[37] HAADF-STEM imaging was performed on an FEI Titan 80–300. EDS analyses were conducted using a probe-corrected FEI Titan G2 80–200, operated at 200 keV and equipped with a SuperX large area windowless X-ray detector array. Transport property measurements were conducted using a standard van der Pauw technique to acquire the in-plane electrical resistivity and Hall coefficient of the compounds in a temperature range of 10–295 K.

Acknowledgements

We acknowledge support from the National Science Foundation under grant DMR-1266217. Grant MRI 0923577 provided funding for the dual beam FIB used to make TEM cross sections. M.F. acknowledges support from the National Science Foundation through CCI grant number CHE-1102637. Sandia National Laboratories is a multi-program laboratory managed and operated by Sandia Corporation, a wholly owned subsidiary of Lockheed Martin Corporation, for the U.S. Department of Energy's National Nuclear Security Administration under contract DE-AC04-94AL85000.

Keywords: kinetic control · layered structures · nanostructures · selenides · van der Waals heterostructures

How to cite: *Angew. Chem. Int. Ed.* **2015**, *54*, 15468–15472
Angew. Chem. **2015**, *127*, 15688–15692

[1] K. Novoselov, D. Jiang, *Proc. Natl. Acad. Sci. USA* **2005**, *102*, 10451–10453.
[2] K. S. Novoselov, A. K. Geim, S. V. Morozov, D. Jiang, Y. Zhang, S. V. Dubonos, I. V. Grigorieva, A. A. Firsov, *Science* **2004**, *306*, 666–669.
[3] A. Koma, K. Ueno, K. Saiki, *J. Cryst. Growth* **1991**, *111*, 1029–1032.
[4] P. Miró, M. Audiffred, T. Heine, *Chem. Soc. Rev.* **2014**, *43*, 6537–6554.
[5] M. Chhowalla, H. S. Shin, G. Eda, L.-J. Li, K. P. Loh, H. Zhang, *Nat. Chem.* **2013**, *5*, 263–275.
[6] Y. Shi, H. Li, L.-J. Li, *Chem. Soc. Rev.* **2015**, *44*, 2744–2756.
[7] C. Tan, H. Zhang, *Chem. Soc. Rev.* **2015**, *44*, 2713–2731.
[8] Y. Min, G. D. Moon, C.-E. Kim, J.-H. Lee, H. Yang, A. Soon, U. Jeong, *J. Mater. Chem. C* **2014**, *2*, 6222.
[9] H. Wang, F. Liu, W. Fu, Z. Fang, W. Zhou, Z. Liu, *Nanoscale* **2014**, *6*, 12250–12272.
[10] T. Niu, A. Li, *Prog. Surf. Sci.* **2015**, *90*, 21–45.
[11] X. Huang, C. Tan, Z. Yin, H. Zhang, *Adv. Mater.* **2014**, *26*, 2185–2203.
[12] R. Lv, J. Robinson, R. Schaak, *Acc. Chem. Res.* **2015**, *48*, 56–64.
[13] M. Pumera, Z. Sofer, A. Ambrosi, *J. Mater. Chem. A* **2014**, *2*, 8981–8987.
[14] A. B. Kaul, *J. Mater. Res.* **2014**, *29*, 348–361.
[15] H. Yuan, H. Wang, Y. Cui, *Acc. Chem. Res.* **2015**, *48*, 81–90.
[16] M. Osada, T. Sasaki, *Adv. Mater.* **2012**, *24*, 210–228.
[17] A. K. Geim, I. V. Grigorieva, *Nature* **2013**, *499*, 419–425.
[18] M. Beekman, C. L. Heideman, D. C. Johnson, *Semicond. Sci. Technol.* **2014**, *29*, 064012.
[19] D. B. Moore, M. Beekman, S. Disch, D. C. Johnson, *Angew. Chem. Int. Ed.* **2014**, *53*, 5672–5675; *Angew. Chem.* **2014**, *126*, 5778–5781.
[20] G. Dittmar, H. Schaefer, *Acta Crystallogr. Sect. B* **1976**, *32*, 2726–2728.
[21] J. Rigoult, C. G. Morosini, A. Tomas, P. Moline, *Acta Crystallogr. Sect. B* **1982**, *38*, 1557–1559.
[22] M. Bayard, M. J. Sienko, *J. Solid State Chem.* **1976**, *19*, 325–329.
[23] L. F. Schneemeyer, A. Stacy, M. J. Sienko, *Inorg. Chem.* **1980**, *19*, 2659–2662.
[24] C. F. van Bruggen, C. Haas, *Solid State Commun.* **1976**, *20*, 251–254.
[25] C. Mande, R. N. Tatil, A. S. Nigavekar, *Nature* **1966**, *211*, 5048.
[26] S. Asanabe, *J. Phys. Soc. Jpn.* **1961**, *16*, 1789.
[27] Y. Zhang, H. Li, L. Jiang, H. Liu, C. Shu, Y. Li, C. Wang, *Appl. Phys. Lett.* **2011**, *98*, 113118.
[28] M. Nath, A. Choudhury, C. Rao, *Chem. Commun.* **2004**, *1*, 2–3.
[29] X. Wang, B. Liu, Q. Wang, W. Song, X. Hou, D. Chen, Y. Cheng, G. Shen, *Adv. Mater.* **2013**, *25*, 1479–1486.
[30] H. S. Im, Y. R. Lim, Y. J. Cho, J. Park, E. H. Cha, H. S. Kang, *J. Phys. Chem. C* **2014**, *118*, 21884–21888.
[31] L. Fister, D. C. Johnson, *J. Am. Chem. Soc.* **1992**, *114*, 4639–4644.
[32] M. Falmbigl, A. Fiedler, R. E. Atkins, S. F. Fischer, D. C. Johnson, *Nano Lett.* **2015**, *15*, 943–948.
[33] E. Hoschek, W. Klemm, *Z. Anorg. Allg. Chem.* **1939**, *242*, 49–62.
[34] H. Terrones, M. Terrones, *J. Mater. Res.* **2014**, *29*, 373–382.
[35] A. Zunger, *Phys. Rev. B* **1979**, *19*, 6001–6009.
[36] M. B. Alemayehu, K. Ta, M. Falmbigl, D. C. Johnson, *J. Am. Chem. Soc.* **2015**, *137*, 4831–4839.
[37] S. Schaffer, B. Schaffer, Q. Ramasse, *Ultramicroscopy* **2012**, *114*, 62–71.

Received: July 4, 2015
Published online: November 6, 2015

